Separations

Water defluoridation: nanofiltration vs membrane distillation

Lucia Moran, Marie Paquet, Katarzyna Janowska, Paul Jamard, Cejna Anna Quist-Jensen, Gabriela Natalia Bosio, Daniel Mártire, Debora Fabbri, and Vittorio Boffa

Just Accepted

Water defluoridation: nanofiltration vs membrane distillation

Lucía I. Moran Ayala,[1] Marie Paquet,[2] Katarzyna Janowska,[2] Paul Jamard,[2] Cejna A. Quist-Jensen,[2]

Gabriela N. Bosio[1], Daniel O. Mártire[1], Debora Fabbri,[3] Vittorio Boffa[2,*]

[1]*Instituto de Investigaciones Fisicoquímicas Teóricas y Aplicadas (INIFTA), CONICET, Universidad Nacional de La Plata, Diagonal 113 y calle 64, 1900, La Plata, Argentina.*

[2]*Department of Chemistry and Bioscience, Aalborg University, Fredrik Bajers vej 7H, 9220 Aalborg, Denmark.*

[3]*Dipartimento di Chimica, Universitá di Torino, Via P. Giuria 5, 10125 Torino, Italy.*

*Correspoinding author: Vittorio Boffa, e-mail: vb@bio.aau.dk

1

Abstract

Nowadays fluoride contamination of drinking water is a major problem for various countries, because high concentrations of fluoride pose a risk of dental and skeletal fluorosis. Over the past years, membrane nanofiltration (NF) has been proposed as convenient defluoridation technology. However, NF cannot be applied to water systems with high fluoride concentration and the disposal of the membrane concentrate remains an issue. In this work, we compared a commercial polyester NF membrane and a polypropylene hollow-fiber membrane distillation (MD) module for their ability to remove fluoride ions from water in the presence of hardness ions and organic fouling agents. The NF membrane can offer more than 10 times higher water productivity than MD, under realistic gradients of temperature and pressure, respectively. Despite that, after reaching a concentration factor of about 3, fouling and scaling caused the flux to drop-to about 80 % respect to its initial value. Moreover, F^- retention decreased from 90% to below 80%, thus providing a permeate of scarce quality. MD was operated in the direct-contact mode on a polypropylene hollow-fiber membrane, which was charged with a hot feed flow (average T = 58 ºC) on one side and a cooled (20 ºC) permeate flow of distilled water on the other side. The concentration of fluoride ion in the permeate was always below the detection limit of our electrode (0.2 ppm), regardless of the fluoride concentration in the feed. Moreover, the MD module showed higher resistance to fouling and scaling than NF and CaF_2 crystals were recovered from the MD concentrate after cooling. These results suggest that the synergic combination of the two techniques might be beneficial for the purification of fluoride-contaminated water systems: MD can be used to further concentrate the NF retentate, thus producing high-purity water and recovering CaF_2 crystals.

Keywords: membrane separation; distillation; fouling; scaling; fluorite crystallization.

2

Introduction

Contamination of drinking water by fluoride is associated with health hazards such as dental and skeletal fluorosis.[1,2] High fluoride concentration in natural water can be caused by geogenic sources (as leaching of fluorine-containing minerals in rocks and sediments) and anthropogenic sources, mainly due to the use of pesticides and to industrial activities. Thus, nowadays fluoride contamination of drinking water is a major problem for various countries,[3] including Argentina, Mexico, United States, Middle East countries, China and India. World Health Organization (WHO) indicates the limits of fluoride concentration in drinking water between 0.5 and 1.0 mg L^{-1} and recommends setting local guidelines at a concentration lower than 1.5 mg L^{-1}.[4,5] Hence, various technologies have been proposed for the abatement and the control of fluoride,[6] such as adsorption, ion exchange, chemical precipitation, and a range of membrane processes encompassing reverse osmosis (RO), nanofiltration (NF), electrodialysis, and really recently membrane distillation (MD). Efficiency and productivity of these processes is governed by different factors, such as raw water characteristics, pressure, temperature, etc.

One of the emerging processes is NF, which has been applied to water defluoridation with promising results at laboratory and pilot scale, over the last decade.[7-20] NF is a pressure-driven process, in which the contaminants are removed by a water-permeable membrane. NF membranes have typically 1-2 nm diameter pores, that is, larger than the size of hydrated ions (e.g. the effective size of hydrated fluoride[21-23] ions is ~0.3 nm). Therefore, their selectivity depends on a combination of steric and charge interactions,[24-26] which allow removing hardness ions and reducing the concentration of monovalent ions (as fluoride). NF membranes have lower ion rejection than reverse osmosis (RO) membranes, but can offer several advantages, such as low operating pressure, high permeability and relatively low costs of investment, operation and maintenance.[26,27] The two main drawbacks of NF membranes are the following: (i) the quality of the produced water is affected by the fluoride

concentration in the feed; (ii) their productivity is reduced by concentration-polarization phenomena. In short, due to the water permeation, salt concentration increases in the vicinity of the membrane surface, thus resulting in an increased salt concentration in the permeate, which corresponds to a decrease in the observed retention. Moreover, scaling and fouling require frequent backwashing and cleaning at the detriment of membrane service time and productivity.

In this context, membrane distillation (MD) has been recently proposed as a possible alternative to NF and RO in desalination[28,29] and defluoridation[30-32] processes. The cross-sectional diagrams of NF and MD are depicted in Figure 1, in order to stress the main differences between the two processes. MD is an emerging technology, which is based on the transport of water vapor through a hydrophobic macroporous membrane. In this case, membrane pores have a size, which is two orders of magnitude larger than the hydrated ions, thus size exclusion and charge interaction do not contribute to the separation mechanism. Indeed, the distillation membrane acts as a barrier between the hot polluted solution and the cold permeate.[33-35] Due to its hydrophobic properties, the membrane is not permeable to water in liquid state, but allows for steam permeation. Mass and heat transfer mechanisms govern steam flux from the hot feed to the cold permeate side of the membrane. The main advantage of MD is the ability to operate at a lower operating feed temperature than conventional distillation and a much lower hydrostatic pressure than NF and RO.[36] Moreover, MD permeability and selectivity are both negligibly affected by the increase of osmotic pressure and concentration polarization phenomena during the feed concentration.[37] On the other hand, temperature polarization has a negative impact on the water productivity of MD systems.
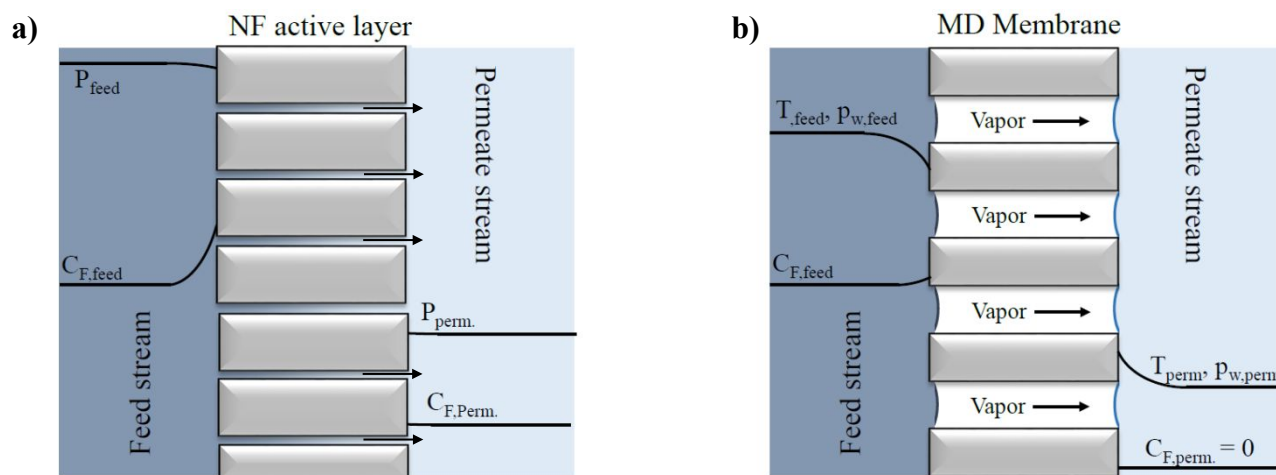
Figure 1. Cross-sectional diagrams of fluoride concentration (C_F), hydraulic pressure (P), water vapor pressure (p_w) and temperature (T) of the feed and permeate side for: (a) NF active layer and (b) MD membrane.

The aim of this work is to assess the advantages and the limits of MD in filtering fluoride-contaminated water by a direct comparison with a benchmark NF module. Hence, two membranes, namely a macroporous hollow fiber polypropylene MD and a microporous polyamide over polysulfone NF membrane,[38] were tested for their ability to remove fluoride ions in the presence of hardness ions and organic fouling agents.

2. Experimental

2.1. Nanofiltration tests

Nanofiltration tests were performed with a cross-flow filtration set-up, which was assembled in our laboratories, over polyester NF membranes (Alfa Laval, $\geq$ 99% rejection of $MgSO_4$ at 2000 ppm, 9 bar, and 25°C. Two disc membranes (totalfiltering area 0.072m²) were sealed in a stainless steel membrane module. Feed was pumped to the membrane by the feed pump (BEVI, IEC 34-1, Sweden).

Permeate mass flow was measured by a balance. Feed pressure was measured before and after the membrane by two pressure transmitters (Danfoss, MBS 4010, Denmark) and an electronic heat sensor (Kamstrup A/S, Denmark) measured feed temperature before membrane module. A rotary lobe pump (Philipp Hilge Gmbh & Co, Novalobe, Germany) controlled the cross-flow rate measured by a microprocessor-based flow rate transmitter (Siemens, MAG 50000). It was adjusted to be 0.17 L s^{-1} for all the experiments. The flow rate of the retentate stream was controlled by a manual valve (Nupro ®). An Agilent ATR FT-IR 630 spectrophotometer with a spectral range 5100-640 cm^{-1} was employed to analyze the NF membrane after being in contact with humic substances. The spectral resolution of the equipment is lower than 2 cm^{-1} and its precision is 0.05 cm^{-1}.

2.2 Membrane distillation tests

Membrane distillation tests were performed on a set-up, which is illustrated elsewhere.[50] The feed was pumped (Cole-Parmer Masterflex L/S) to a heater (Haake K20) and afterwards into the lumen side of the membrane module, and then it returned to a feed tank. The permeate was pumped (Cole-Parmer Masterflex L/S) to a cooler (Julabo FP50) and into the module in the shell side in countercurrent flow with respect to the feed. The increase of permeate volume was scrutinized by a balance (A&D Company Limited FZ-300i). The temperature was monitored in feed and permeate at inlet and outlet of the module (Ludwig Schneider, Type 13100). The membrane module used for all experiments was made using Membrana Accurel® PP S6/2 hollow fiber membranes. The outer diameter of the hollow fiber was 2.5 mm, inner diameter was 1.6 mm and thickness was 0.45 mm. The porosity of the membranes was 73% with a pore size of 0.2 μm. The total membrane surface area of the 5 fibers was 0.010 m^2.

2.3 Feed solutions and water analysis

Pure water permeability was measured by filtering deionized water Milli-Q produced (Resistivity > 18 MΩ cm). For NF and MD tests a model fluoride water solution was prepared and analyzed as follow. A Thermo Scientific™ Dionex™ ED40 instrument equipped with a conductimeter detector was used to measure the anion concentration. Anions were analyzed with an AS9HC column and a K_2CO_3 solution (9 mM) as eluent at a flow rate of 1 mL min^{-1}. A PerkinElmer® Optima 7000 DV ICP-Optical Emission Spectrometer (Shelton, CT, USA) equipped with WinLab™ 32 for ICP Version 4.0 software was used for measurement of cations. Conductivity was measured with SevenMultiTM S70-K benchtop (± 0.5% accuracy). Fluoride concentration was measured with a fluoride selective electrode model FOO1503 (Van London, Phoenix). The X-rays diffraction (XRD) patterns of the filtered MD concentrate was acquired over a PANanalytical Empyrean diffractometer, operating at 45 kV and 40 mA, with Cu Kα radiation. The composition in Table 1 was used to simulate precipitation of salts during the concentration of the polluted feed water. The precipitation was simulated through the geochemical software PHREEQC interactive-version 3.[39] A so-called "REACTION" feature in the software was utilized to remove a specified amount of water in a given number of steps. The output of the software provides information on which salts that precipitates and in which amounts, etc. Temperature, pH and redox potential of the polluted water in the simulations has been assumed to 25 °C, 6.9 and 4 pe, respectively.

3. Results and discussion

3.1. Water productivity

Figure 2 allows comparing the permeate flux (J_W, L m^{-2} h^{-1}) of the NF and MD membranes, when

deionized water (resistivity $\geq$ 18 MΩ cm) is filtered at realistic gradients of pressure and temperature,

respectively. A water permeability of 6.5 ± 0.1 L (m^2 h bar)$^{-1}$ for the NF membrane was measured by

fitting the experimental data in Figure 2a. This value is consistent with the water permeability reported

in literature for the other commercial NF membranes,[40-48] thus making this module a good basis of

comparison for the MD membrane. The water fluxes achieved by the MD membrane (Figure 2b) range

between 2 and 4.5 L (m^2 h)$^{-1}$ and are also in line with the literature values.[49] In general, the permeate

flux can be increased by increasing the temperature gradient i.e. the vapor pressure gradient across the

membrane. Increasing the crossflow velocity also results in an increased flux, due to the smaller

temperature drop along the membrane fiber (horizontal lines in Figure 2b). At an average feed

temperature of 58 °C and permeate temperature of 20 °C the MD membrane can produce a flux of 4.5

L (m^2 h)$^{-1}$, while the NF membrane has a water flux of about 60 L (m^2 h)$^{-1}$ at a transmembrane pressure

(ΔP) of 9 bar. Therefore, the MD membrane permits to obtain water fluxes, which are one order of

magnitude lower than those achieved by NF, i.e. the MD membrane requires more than 10 times larger

area to filter the same amount of water than its NF counterpart does.

Nevertheless, real water systems are complex mixtures of inorganic ions, organic molecules and

often contain biological materials. Therefore, the two membranes should be compared for their

permeability and their selectivity towards fluoride ions, in such type of systems. Moreover, they should

be able to maintain their perm-selectivity during filtration. For this reason, a model water system

simulating fluoride-contaminated water was prepared and filtered over both the commercial NF

membrane and the MD membrane. The chemical and physical properties of this water system are

reported in Table 1. Such water system had a total conductivity of 0.54 mS cm^{-1}, pH 6.9, and a total

hardness of 4.45 meq L^{-1}. The concentrations of fluoride and humic substances were 15.0 and 5 mg L^{-1},

respectively. The filtration performances of the two membranes during the concentration of the feed

solution were investigated by measuring their permeate flux (J_w), and by comparing retenate and

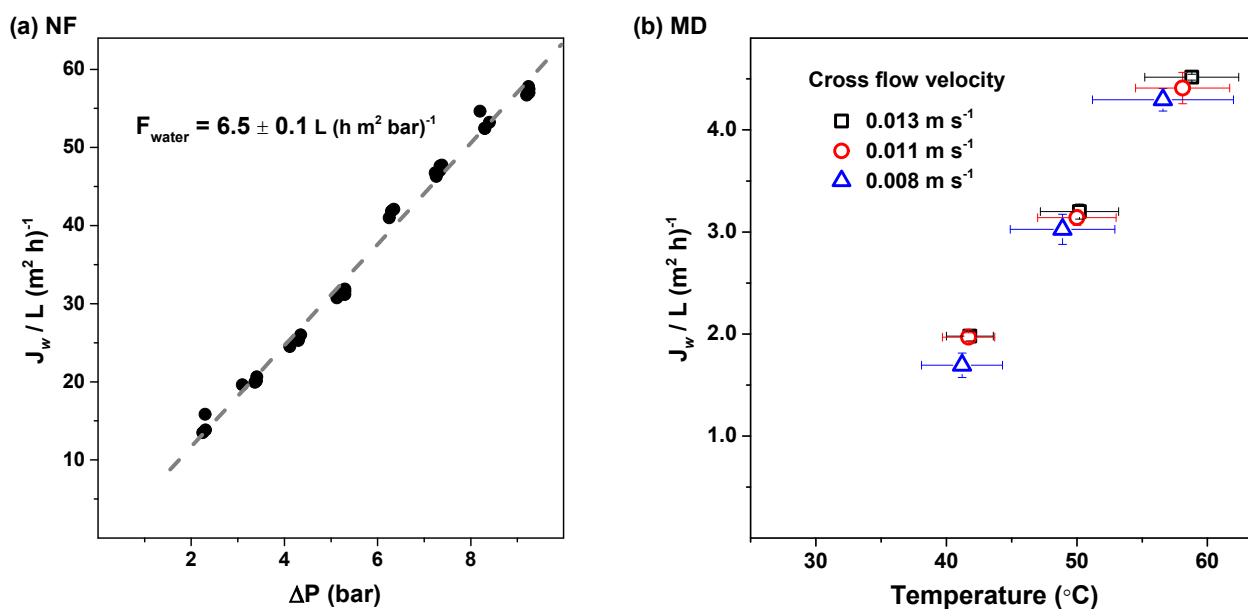permeate for their concentration of fluoride ions, dissolved ions, and humic substances.

Figure 2. Filtration of deionized water. (a) Permeate flux (J_w) as a function of membrane overpressure in NF; the linear fitting of the experimental data (dashed line) was used to calculate the membrane water permeance (F_{water}). (b) J_w of MD as a function of feed temperature: the horizontal bars and bullets indicate the temperature at the two membrane extremes and the average temperature, respectively; vertical bars indicate the standard deviation over 4 measurements; the permeate had an average temperature of 20 °C and the same cross flow velocity of the feed.

Table 1. Composition and physical properties of the model water system used for filtration tests.

		Anions		cations	
Conductivity (mS cm^{-1})	0.54	F$^-$ (mg L^{-1})	15.0	K$^+$ (mg L^{-1})	1.55
pH	6.9	Cl$^-$ (mg L^{-1})	24.1	Na$^+$ (mg L^{-1})	21.6
Hardness (meq L^{-1})	4.45	SO$_4^{2-}$ (mg L^{-1})	16.6	Mg^{2+} (mg L^{-1})	5.88
Humic acid (mg L^{-1})	5.0	NO$_3^-$ (mg L^{-1})	24.1	Ca^{2+} (mg L^{-1})	79.24

3.2 Fluoride selectivity

The fluoride concentration in the feed and in the permeate of the NF membrane was measured by a specific electrode and plotted as a function of the concentration factor (initial feed volume/volume of the feed solution during filtration) in Figure 3a. When filtration started, a fluoride concentration in the permeate ($C_{F,permeate}$) of 1.7 ppm was measured, corresponding to a selectivity (1- $C_{F,permeate}$/ $C_{F,feed}$) of about 89%. The quality of the NF permeate strongly changes during the concentration of the model water system. For instance, $C_{F,permeate}$ is about 2.4 ppm for a feed concentration factor of 2 and > 3ppm for a feed concentration factor of 3. Such permeate is not suitable for human consumption. This result is not surprising, since NF membranes are known to be partially permeable to F$^-$ ions. Therefore, they are neither suitable to filter feeds with a high concentration of fluoride ions, nor to achieve high concentration factors. Moreover, the membrane selectivity decreases during filtration, as shown by the blue triangles in Figure3a. The decrease in the F$^-$ retention with increasing the feed concentration factor can be explained by the well-known concentration polarization phenomena, which becomes more relevant at high ion concentration.

Despite the low water productivity, MD shows a higher ability to decrease the concentration of fluoride ions than NF. Indeed the concentration of the F$^-$ ions remained below the detection limit of our

electrode (0.2 ppm) even after reaching a concentration factor of 9 (Figure 3b). In order to appreciate

the selectivity of the MD membrane, model solutions of with F^- concentration ranging from 10 to 1000

ppm were prepared by dissolving NaF in deionized water and tested with the same ΔT and initial feed

and permeate volumes of the previous experiment. The fluoride concentration in the permeate tank and

the permeate flux are reported in Figure 4 as a function of the fluoride concentration in the feed. These

data show that the membrane can completely retain F^- ions also for feeds with concentrations as high as

1 g L^{-1}. Moreover, in the absence of hardness ions, the permeate flux is not affected by the F^-

concentration in the feed solutions.

3.3 Scaling and salt retention

By observing the data points in Figure 3, we can notice that surprisingly the concentration of the

F^- ions in the feed tank does not increase linearly with the feed concentration factor, but it reaches a

plateau, which corresponds to about 20 ppm (from a concentration factor =3) for NF and to about 40

ppm (from a concentration factor =5) for MD. This can be explained by considering the hardness of our

water system (4.45 meq L^{-1}) and the scarce solubility of CaF_2, which is 24.2 ppm at 25 °C.[54] Therefore,

we can expect that CaF_2 crystals will form during filtration and will eventually precipitate on the

membrane surface, in the feed tank or in the tubing.

Hardness ions, as Ca^{2+} and Mg^{2+}, are notorious scaling agents, because they forms scarcely soluble

salts with F^- and several other anions as CO_3^{2-} and SO_4^{2-}. Precipitation of $CaCO_3$ and other scaling salts

can be indirectly observed by measuring the conductivity of the feed and of the permeate, since it gives

an estimation of the total free ions in solution. During NF a constant conductivity is reached for

concentration factors higher than 3 (Figure 5a), as for the fluoride ions (Figure 3a). Scaling is negative

for the NF filtration performances, since it can reduce the permeate flux and screen the negative charge

11

of the membrane surface,[55] thus reducing the retention of the negative F$^-$ ions. On the contrary, the high temperature of the MD feed solution (~58 °C) hinders the precipitation of inorganic salts and the concentration of the free ions at a concentration factor of 8 (Figure 5b) is nearly 3 times higher that measured for the NF membrane (Figure 5a).
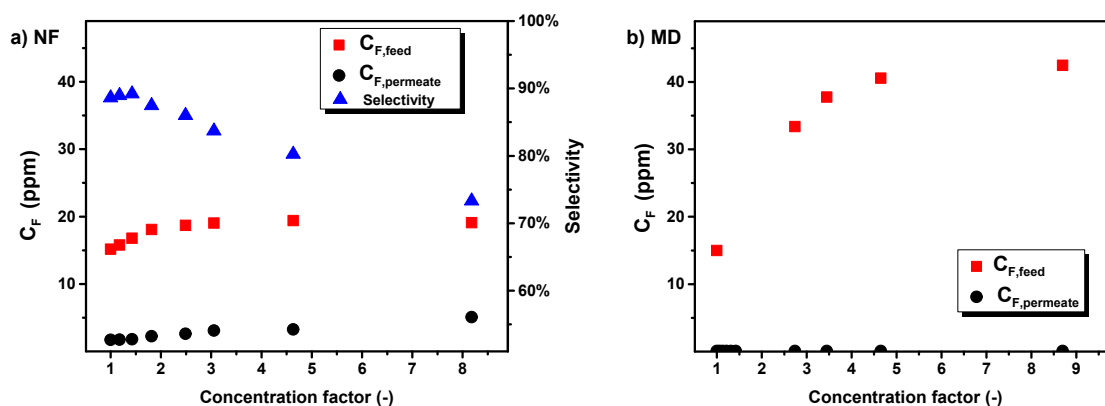

Figure 3. Fluoride concentration in the feed and in the permeate during concentration of the model water system in Table 1. (a) Nanofiltration (NF) was performed at ΔP = 9 bar, cross flow rate of 0.17 L s^{-1}. (b) Membrane distillation (MD) was performed at a cross-flow velocity of 0.013 m s^{-1} and the average temperatures of the feed side and side were 58 °C and 20 °C, respectively; the initial volumes of feed and permeate were 2.4 L and 0.40 L, respectively.
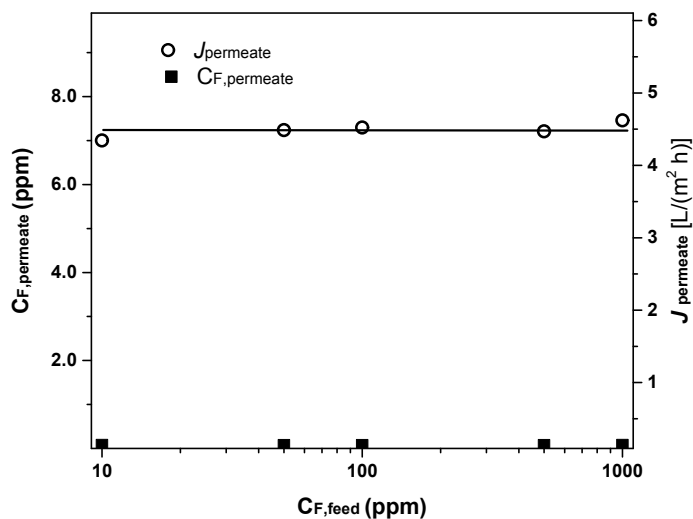
Figure 4. Filtration of deionized water contaminated with fluorine: measured fluoride concentration in the permeate ($C_{F,permeate}$) and permeate flux (J_W) as a function of the fluoride concentration in the feed tank ($C_{F,feed}$) for the MD membrane. The experiment was performed at a cross-flow velocity of 0.013 m s^{-1} and the average temperatures of the feed side and permeate side were 58 °C and 20 °C, respectively; the initial volumes of feed and permeate were 2.4 L and 0.40 L, respectively.

Figure 5a also shows that the NF membrane can only partially retain the dissolved ions. This is not surprising since NF membranes are known to have higher rejection towards polyvalent than for monovalent ions. The total salt retention, here estimated from the ratio between the conductivity of the permeate and of the retentate, is about 57% when filtration started. Then, a steady decline in salt retention is observed, which is probably due to the polarization phenomena and to the precipitation of salts crystals on the membrane surface, as discussed above for the retention towards fluoride ions. On the contrary, the permeation of inorganic ions is negligible for the MD membrane, also when high concentration factors are reached (Figure 5b). Here, it should be stressed that, while the retention of the potentially harmful fluoride ions is desired, the composition of the MD permeate is not suitable for

human consumption, due to its low salinity. Therefore, when MD is used for the production of drinking water, additional costs should be considered to adjust the permeate salinity.
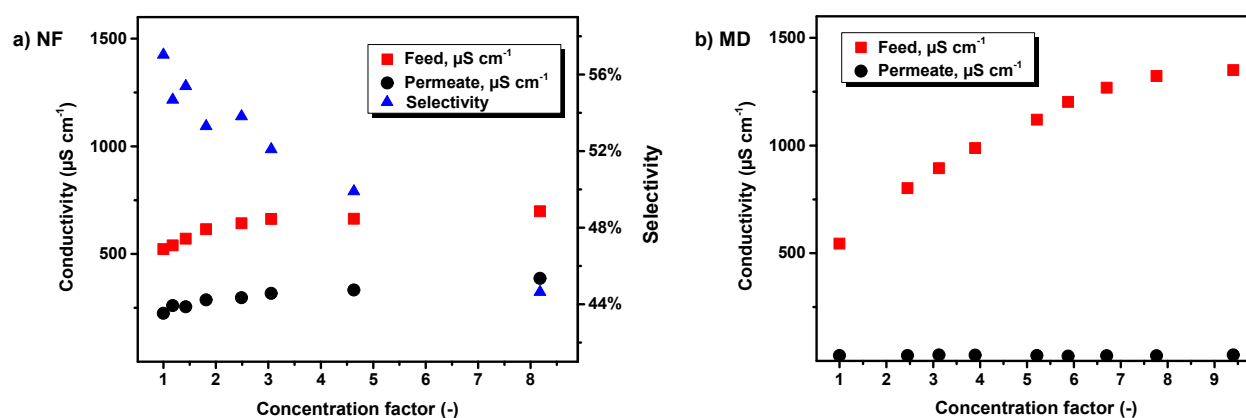

Figure 5. Conductivity of the feed and of the permeate during concentration of the model water system in Table 1. (a) Nanofiltration (NF) was performed at ΔP = 9 bar and crossflow rate of 0.17 L s^{-1}. (b) Membrane distillation (MD) was performed at a cross-flow velocity of 0.013 m s^{-1} and the average temperatures of the feed side and permeate side were 58 °C and 20 °C, respectively; the initial volumes of feed and permeate were 2.4 L and 0.40 L, respectively.

3.4 Fouling and permeate flux

As scaling is often combined with organic fouling, our model systems was sparked with humic substances (HA) at a concentration of 5 mg L^{-1}. HA molecule are common foulants, which can bind to membrane surface, blocking the membrane pores. The concentration of humic acid in the feed and in the permeate was investigated by spectrophotometric analysis. A_{254} is the absorbance of the solution at 254 nm, which is a good indicator for the concentration of humic substance in our model system. The data reported in Figure 6 point out that both membranes can completely retain HA molecules as their permeates have $A_{254} \sim 0.0$, regardless of the concentration factor. However, the light absorption A_{254} of

the NF concentrate in the feed thank shows an unexpected trend: it decreases during filtration. The

filtration was stopped after reaching a concentration factor of ~ 8. At this point, the membrane surface

was inspected, revealing a brown deposit, which can be observed in the insert of Figure 6a.

Again, the MD membrane has a different behavior compared to NF. The HA concentration in the

MD feed thank increases during concentration (Figure 6b). However, this trend is not linear and

therefore it cannot be excluded that part of the HA molecules start being adsorbed on the membrane

surface at high concentration factors. Indeed, the amphiphilic character of the humic substances allow

them to interact with both the highly hydrophilic NF and the hydrophobic MD membranes
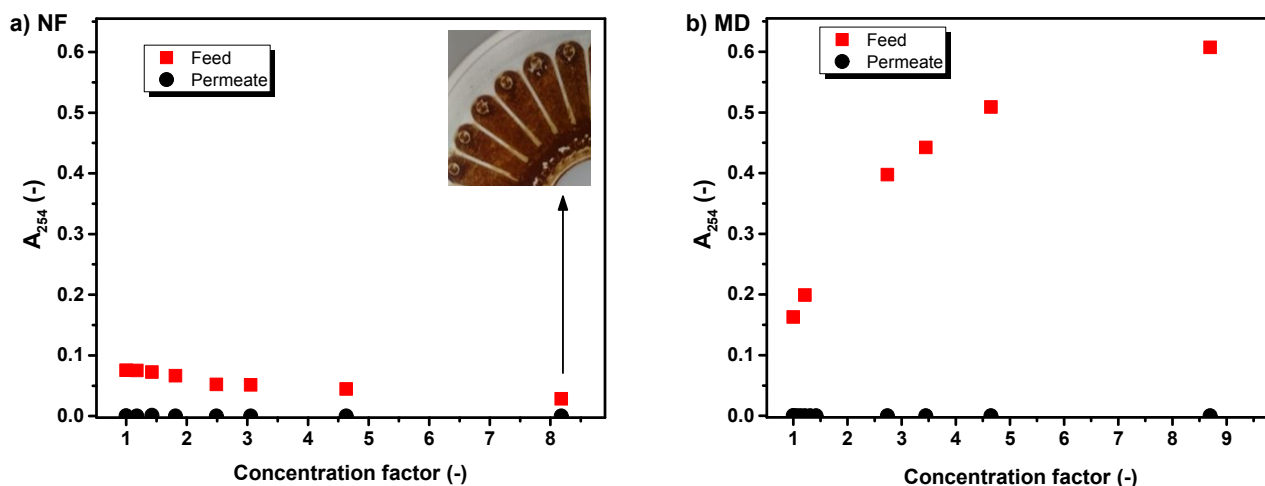
Figure 6. Light absorbance at 254 nm (A_{254}) of the feed and of the permeate during concentration of

the model water system in Table 1. (a) Nanofiltration (NF) was performed at $\Delta P = 9$ bar, cross flow

rate of 0.17 L s^{-1}; the picture in the insert shows a portion of the surface of the polymeric NF

membrane at the end of the experiment. (b) Membrane distillation (MD) was performed at a cross-flow

velocity of 0.013 m s^{-1} and the average temperatures of the feed side and permeate side were 58 °C and

20 °C, respectively; the initial volumes of feed and permeate were 2.4 L and 0.40 L, respectively.

Figure 7 depicts the permeate flux as a function of the concentration factor for (a) the NF membrane and (b) the MD membrane. Both membranes show a flux decline during filtration. However, since the two membranes have a different interaction with the humic acid and function under different driving forces, they show different fouling behaviour. As it is observed in Figure 6a, the permeate flux of the NF membrane at the beginning of the filtration is 42 L $(m^2 h)^{-1}$ at $\Delta P = 9$ bar, that is only 72% of that measured for the demineralized water. This can be ascribed to an increase of the osmotic pressure across the membrane, due to the high ionic strength of the feed solution, and to the membrane fouling, which in our system is caused by the accumulation of humic substances on the surface of the membrane. Moreover, when a concentration factor of 3 is reached, the permeate flux of the NF membrane has an abrupt drop, and at a concentration factor of ~ 8 J_W is equal to only 14 L $(m^2 h)^{-1}$. This change is probably due to the scaling of the membrane surface, as we indirectly observed salt precipitation from the measurement of the fluoride concentration and the conductivity of the NF concentrate in Figure 3a and Figure 5a, respectively. The permeate flux decrement for the MD membrane is less pronounced compare to the NF membrane. When compared to the filtration of demineralized water, J_w is equal to 90% at the beginning of the filtration, and to 55% when a concentration factor of about 9 is reached.
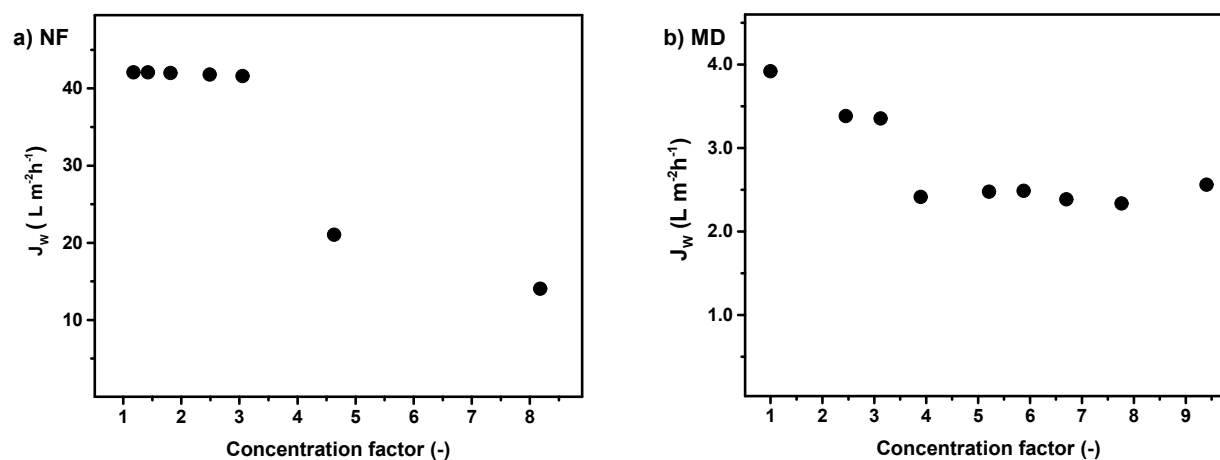
Figure 7. Permeate flux (J_W) during concentration of the model water system in Table 1. (a) Nanofiltration (NF) was performed at $\Delta P = 9$ bar, cross flow rate of 0.17 L s^{-1}; the picture in the insert shows a portion of the surface of the polymeric NF membrane at the end of the experiment. (b) Membrane distillation (MD) was performed at a cross-flow velocity of 0.013 m s^{-1} and the temperatures of the feed side and permeate side were 58 °C and 20 °C, respectively; the initial volumes of feed and permeate were 2.4 L and 0.40 L, respectively.

3.5 Salts in the MD concentrate

While most the HA molecules and the precipitated salts deposit on the NF membrane surface during filtration, those remain in dispersed in the feed solution when the model water system is treated by MD. Thus, after the filtration experiment, the MD concentrate was let to cool at room temperature. A picture of it is reported in the insert of Figure 8. At the bottom of the flask, we can see a brown precipitate, which must consists of insoluble humate salts (e.g. calcium and magnesium humate[56,57]) and mineral crystals. The precipitate was filtered over a paper filter and analyzed at the X-ray diffractoremeter. The diffraction patter (Figure 8) was used to investigate the composition of the salt

17

crystals precipitated after cooling the MD concentrate. Such analysis was performed with the "search

and match" function of the software HighScore Plus (PANalytical 2017). The peaks of our

diffractogram were compatible with only two types of crystals: fluorite (CaF_2 [ref. 58], peaks at $2\theta =$

28.57°, 47.52°, and 56.4°) and calcite ($CaCO_3$ [ref. 59,60] or $Ca_{0.94}Mg_{0.06}CO_3$ [ref. 60], peaks at $2\theta =$

29.5°, 31.6°, 36.1°, 39.6°, 43.3°, 47.2°, 47.6°, 48.6°, and 57.5°). The reference diffractograms of other

minerals cannot be matched with the peaks in Figure 8. This is consistent with the solubility product

constants (at 25 °C)[61] of the salts that can be formed by concentration of the model water system in

Table 1: CaF_2 1.7 10^{-14}, $CaCO_3$ 4.7 10^{-9}, MgF_2 8 10^{-8}, $MgCO_3$ 4.0 10^{-5}, $CaSO_4$ 2.5 10^{-5}.
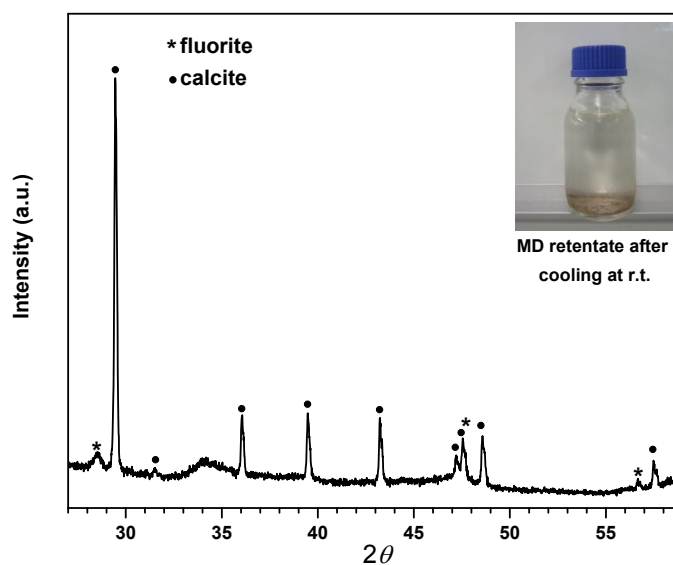
Figure 8. XRD pattern of the crystals in the MD concentrate, which showed in the insert picture.

The low solubility of fluorite (CaF_2) makes it possible to aim for its selective recovery from MD

concentrate, as shown by the simulation in Figure 9. If we consider a mixture with the composition

18

reported in Table 1, fluorite is the first mineral salt that precipitate during concentration. The filtration can be stopped before the formation of a significant amount of calcite, thus allowing for the recovery of pure fluorite crystals from the MD concentrate.
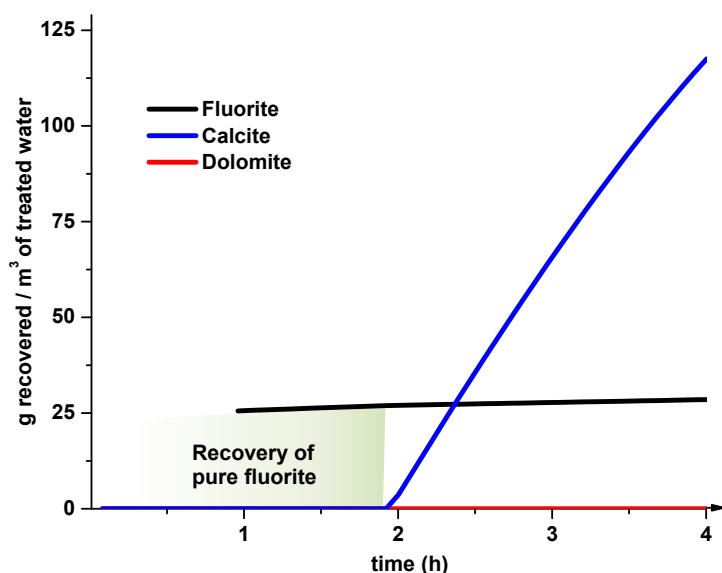
Figure 9. MD can be used to recover pure fluorite upon partial concentration of fluoride-contaminated water. The *x*-axes indicates the filtration time for 1 m^3 of a fluoride-contaminated water (Table 1) over a MD membrane of the same type which was used in our experiment and an area of 50 m^2. The *y*-axes indicates the amount of salt the can be recovered from the concentrate.

Conclusions

In summary, both NF and MD allow for the rejection of fluoride ions in solution. However, these two processes are based on different mechanisms of permeation and selectivity, and thus they show different performances during concentration of fluoride-contaminated water. The NF membrane is

partially permeable to the fluoride ions and therefore it is not suitable to treat streams with high fluoride concentration and at high concentration factors the permeate might have a fluoride concentration not suitable for human consumption. However, it has much higher water productivity than the MD unit, even after the membrane surface underwent scaling and fouling.

The most important feature of MD is that the feed quality remains constant over all the filtration time and the fluoride concentration in our permeate was below the detection limit of our electrode (0.2 ppm), even after reaching a concentration factor of 9. MD has higher resistance to fouling and scaling than NF. Moreover, it does not require high pressure and solar heat or waste heat can be exploited to generate a vapor pressure gradient across the membrane. The main drawbacks of MD has been proven to be: (i) the low water productivity and (ii) the scarce salinity of the permeate, which must be increased at a level save for human consumption. However, such problems are already faced by the current RO installations.

The results here reported suggest that the synergic combination of the two techniques can be an interesting solution to treat fluoride-contaminated water. At first, NF can be used to purify water until the concentration of fluoride ion in the permeate is compatible with the local requirements for drinking water, or until fouling and scaling make inconvenient to continue the concentration process, even with frequent backwashing. Indeed, NF membranes are partially permeable to fluoride ions and the quality of the produced drinking water deteriorates during concentration. Therefore, the NF concentrate can be further treated by MD. Pre-concentration by NF will be beneficial for the MD process by reducing the energy consumption for the heating and the membrane area. Highly pure CaF_2 can be crystallized by cooling the MD concentrate, and eventually exploited in industrial processes, as the production of hydrogen fluoride. Moreover, the permeates of the NF and MD module can be mixed to obtain a high quality drinking water, with the desired concentration of fluoride ions and dissolved minerals.

References

1. Choubisa, S.L.; Fluorosis in some tribal villages of Dungapur district of Rajasthan, India. *Fluoride*, **1997**, *30*, 223–228.

2. Xu, R.Q.; Wu, D.Q.; Xu, R.Y. Relations between environment and endemic fluorosis in Hohot region, Inner Mongolia. *Fluoride*, **1997**, *30*, 26–28.

3. Ali, S.; Thakur, S.K.; Sarkar, A.; Shekhar S.; Worldwide contamination of water by fluoride. *Environ. Chem. Lett.* **2016**, *14*, 291-315.

4. WHO, Guidelines for Drinking-Water Quality. First addendum to third ed. vol. 1. Recommendations, **2006**, WHO.

5. Murray, J.J. Appropriate use of fluorides for human health. Geneva, **1986,** World Health Organization.

6. S. Ayoob; A. K. Gupta, V. T. Bhat, A conceptual overview on sustainable technologies for the defluoridation of drinking water*, Crit. Rev. Env. Sci. and Tech.* **2008**, *38*, 401-470.

7. Ben Nasr, A.; Charcosset, C.; Ben Amar, R.; Walha, K. Defluoridation of water by nanofiltration, *J. Fluorine Chem.* **2013**, *150*, 92–97.

8. Boussouga, Y.A.; Lhassani, A. Modeling of fluoride retention in nanofiltration and reverse osmosis membranes for single and binary salt mixtures, *Desalination Water Treat.*, **2017**, *95*, 162-169.

9. Owusu-Agyeman, I.; Jeihanipour, A.; Luxbacher, A.T.; Schafer, A I.; Implications of humic acid, inorganic carbon and speciation on fluoride retention mechanisms in nanofiltration and reverse osmosis, *J. Membrane Sci.* **2017**, *528*, 82-94.

10. Harahsheh, M.; Hussain, Y. A.; Al-Zoubi, H.; Batiha, M.; Hammouri, E. Hybrid precipitation-nanofiltration treatment of effluent pond water from phosphoric acid industry, *Desalination*, **2017,** *406*, 88-97.

11. Shen, J.J.; Richards, B.S.; Schafer A. I.; Renewable energy powered membrane technology: Case study of St. Dorcas borehole in Tanzania demonstrating fluoride removal via nanofiltration/reverse osmosis, *Sep. Purif. Technol.*, **2016**, *170*, 445-452.

12. Shen, J. J.; Schafer, A. I. Factors affecting fluoride and natural organic matter (NOM) removal from natural waters in Tanzania by nanofiltration/reverse osmosis, *Sci. Total Environ.*, **2015**, *527* 520-529.

13. Shen, J. J.; Schafer, A. I. Removal of fluoride and uranium by nanofiltration and reverse osmosis: A review, *Chemosphere*, **2014**, *117*, 679-691.

14. Xi, B.D.; Wang, X.W.; Liu, W. J.; Xia, X.F.; Li, D.S.; He, L.S.; Wang, H.M.; Sun, W.J.; Yang T.X.; Tao, W. Fluoride and Arsenic Removal by Nanofiltration Technology from Groundwater in Rural Areas of China: Performances with Membrane Optimization, *Sep. Sci. Technol.*, **2014**, *49*, 2642-2649.

15. I. Bejaoui, A. Mnif, B. Hamrouni, Performance of Reverse Osmosis and Nanofiltration in the Removal of Fluoride from Model Water and Metal Packaging Industrial Effluent, Sep. Sci. Technol., **2014**, *49*, 1135-1145.

16. Chakrabortty, S.; Roy, M.; Pal P. Removal of fluoride from contaminated groundwater by cross flow nanofiltration: Transport modeling and economic evaluation, *Desalination*, **2013**, *313*, 115-124.

17. J. Hoinkis, S. Valero-Freitag, M.P. Caporgno, C. Patzold, Removal of nitrate and fluoride by nanofiltration - a comparative study, Desalination and Water Treatment, 30 (2011) 278-288.

18. I. Bejaoui, A. Mnif, B. Hamrouni, Influence of operating conditions on the retention of fluoride from water by nanofiltration, Desalination and Water Treatment, 29 (2011) 39-46.

19. Wang, X.W.; Xi, B.D.; Huo, S.L.; Liu, W.J.; Sun, W.J.; Li, D.S.; Yu, H.B.; Ma, W.F.; Liu, H.L. Performances comparison of reverse osmosis and nanofiltration application to defluorination from groundwater: influence factors and fouling analysis, *Fresenius Environ. Bull.*, **2011**, *20*, 3141-3151.

20. Padilla, A.P.; Saitua, H. Performance of simultaneous arsenic, fluoride and alkalinity (bicarbonate) rejection by pilot-scale nanofiltration, *Desalination*, 2010, *257* 16- 21.

21. Nightingale, E.R. Phenomenological theory of ion solvation. Effective radii of hydrated ions, J. Phys. Chem. **1959**, *63*, 1381–1387.

22. Zhou, J.; Lu, X.; Wang, Y.; Shi, J. Molecular dynamics study on ionic hydration, *Fluid Phase Equilib.* **2002**, *194–197*, 257–270.

23. M.Y. Kiriukhim, K.D. Collins, Dynamic hydration numbers for biologically important ions, *Biophys. Chem.* 99 (2002) 155–168.

24. Farsi, A.; Malvache, C.; De Bartolis, O.; Magnacca, G.; Kristensen, P. K.; Christensen, M. L.; Boffa V., Design and fabrication of silica-based nanofiltration membranes for water desalination and detoxification, *Microporous Mesoporous Mater.*, **2017**, *237*, 117-126.

25. Farsi, A.; Boffa, V.; Christensen, M. L. Electroviscous effects in ceramic nanofiltration membranes, *ChemPhysChem*, **2015**, *16*, 3397-407.

26. Farsi, A.; Boffa, V.; Qureshi, H.F.; Nijmeijer, A.; Winnubst, L.; Christensen, M. L.Modeling water flux and salt rejection of mesoporous γ-alumina and microporous organosilica membranes, J. Membrane Sci., **2014**, *470*, 307–315.

27. Diawara, C. K. Nanofiltration Process Efficiency in Water Desalination, *Sep. Purif. Rev.*, **2008**, *37*, 302–324.

28. Qtaishat, M.R.; Banat, F. Desalination by solar powered membrane distillation systems, *Desalination* **2013**, *308*, 186-197.

29. Quist-Jensen, C.A.; Ali, A.; Mondal, S.; Macedonio, F.; Drioli, E. A study of membrane distillation and crystallization for lithium recovery from high-concentrated aqueous solutions, J. *Membrane Sci.* **2016**, *505*, 167–173.

30. Hou, D. Y.; Wang, J.; Wang, B. Q.; Luan, Z. K.; Sun X. C.; Ren, X. J. Fluoride removal from brackish groundwater by direct contact membrane distillation, Water Sci. Technol., **2010**, *61*, 2178-3187.

31. Hou, D.; Wang, J.; Zhao, C.; Wang, B.; Luan, Z.; Sun X. Fluoride removal from brackish groundwater by direct contact membrane distillation, *J. Environ. Sci.*, **2010**, *22*, 1860–1867.

32. Boubakri, A.; Bouchrit, R.; Hafiane, A.; Al-Tahar Bouguecha, S. Fluoride removal from aqueous solution by direct contact membrane distillation: theoretical and experimental studies, Environ. Sci. Poll. Research, **2014**, *21*, 10493-10501.

33. Qtaishat, M.; Rana, D.; Matsuura, T.; Khayet, M. Effect of surface modifying macromolecules stoichiometric ratio on composite hydrophobic/hydrophilic membranes characteristics and performance in direct contact, *AIChE* **2009**, *55*, 3145-3151.

34. Qtaishat, M.; Khayet, M.; Matsuura, T. Novel porous composite hydrophobic/hydrophilic polysulfone membranes for desalination by direct contact membrane distillation, *J. Membrane Sci*. **2009**, *341*, 139-148.

35. Qtaishat, M.; Matsuura, T.; Khayet, M.; Khulbe, K.C. Comparing the desalination performance of SMM blended polyethersulfone to SMM blended polyetherimide membranes by direct contact membrane distillation, *Desalination Water Treat.* **2009**, *5*, 91-98.

36. Boubakri, A.; Hafiane. A.; Al Tahar Bouguecha, S. Application of response surface methodology for modeling and optimization of membrane distillation desalination process, J. *Ind. Eng. Chem.*, **2014**, *20*, 3163-3169.

37. Ali, A., Macedonio F.; Drioli E.; Aljlil S.; Alharbi, O. A. Experimental and theoretical evaluation of temperature polarization phenomenon in direct contact membrane distillation, *Chem. Eng. Res. Design* **2013**, *91*, 1966–1977.

38. Meschke, K.; Daus, B.; Haseneder, R.; Repke, J.-U. Strategic elements from leaching solutions by nanofiltration – Influence of pH on separation performance, *Sep. Purif. Technol.* **2017**, *184,* 264–274.

39. Parkhurst, D.L.; Appelo, C.A. Description of Input and Examples for PHREEQC Version 3—A Computer Program for Speciation, Batch-Reaction, One-Dimensional Transport, and Inverse Geochemical Calculations. Available online: http://pubs.usgs.gov/tm/06/a43

40. FILMTEC™ XLE-2521 Membranes, Form No. 609-00349-0706. www.lenntech.com/Data-sheets/Dow-Filmtec-XLE-2521.pdf

41. FLUID SYSTEMS® TFC®-ULP® 4" ELEMENT, KOCH membrane system, www.lenntech.com/Data-sheets/Koch-Fluid-Systems-TFC-4040-ULP-L.pdf

42. Toray Membrane Product, www.toraywater.com/products/ro/pdf/TMG.pdf

43. Hydranautics Corporate http://www.membranes.com/docs/4inch/ESPA4-4040.pdf

44. FILMTEC Membranes, Nanofiltration Produces Sparkling Clean Water for Swedish Resort

Community, Form No. 609-00379-0503,

http://msdssearch.dow.com/PublishedLiteratureDOWCOM/dh_0047/0901b803800478f5.pdf?filepath=

liquidseps/pdfs/noreg/609-00379.pdf&fromPage=GetDoc

45. FILMTEC™ Membranes, FILMTEC NF90-400 Nanofiltration Element, Nanofiltration Elements

for Commercial Systems, Form No. 609-00345-0406, http://www.lenntech.com/Data-sheets/Dow-

Filmtec-NF90-400.pdf

46. CK Series, Water Softening NF Elements (Cellulose Acetate), GE water &process technology,

https://www.gewater.com/kcpguest/salesedge/documents/Fact%20Sheets_Cust/Americas/English/FS12

68EN.pdf

47. Hydranautics Corporate http://www.membranes.com/docs/8inch/ESNA1-LF-LD.pdf

48. Product Guide for Spiral-Wound RO & NF Elements, CSM,

http://www.csmfilter.com/csm/upload/RO_Catalogue/CSM%20RO%20Catalog_Eng_Final_DavidK_1

1.7.12.pdf

49. Ullah, R.; Khraisheh, M.; Esteves, R.J.; McLeskey, J.T.; AlGhouti, M.; Gad-El-Hak, M.; Tafreshi,

H.V. Energy efficiency of direct contact membrane distillation, *Desalination* **2018**, *433* 56-67.

50. C.A. Quist-Jensen, J.M. Sørensen, A. Svenstrup, L. Scarpa, T.S. Carlsen, H.C. Jensen, L.

Wybrandt, M.L. Christensen, Membrane crystallization for phosphorus recovery and ammonia

stripping from reject water from sludge dewatering process, *Desalination*, in press

https://doi.org/10.1016/j.desal.2017.11.034.

51. Perez Padilla, A.; Saitua, H. Performance of simultaneous arsenic, fluoride and alkalinity

(bicarbonate) rejection by pilot-scale nanofiltration, *Desalination* **2010**, *257*, 16–21.

26

52. Richards, L.A.; Richards, B.S.; Rossiter, H.M.A.; Schäfer, A.I. Impact of speciation on fluoride, arsenic and magnesium retention by nanofiltration/reverse osmosis in remote, Australian communities, *Desalination* **2009**, *248*, 177–183.

53. Shen, J.; Schäfer, A. Removal of fluoride and uranium by nanofiltration and reverse osmosis: A review. *Chemosphere* **2014**, *117*, 679–69.

54. McCann, H. G. The solubility of fluorapatite and its relationship to that of calcium fluoride. Arch Oral Biol **1968**, *13*, 987–1001.

55. Tu, K.L.; Chivas, A.R; Nghiem, L.D.; Effects of membrane fouling and scaling on boron rejection by nanofiltration and reverse osmosis membranes, *Desalination* **2011**, *279*, 269–277.

56. Kříženecká, S.; Hejda, S.; Machovič, V.; Trögl, J. Preparation of iron, aluminium, calcium, magnesium, and zinc humates for environmental applications, *Chemical Papers*, **2014**, *68*, 1443–1451.

57. Savarino, P.; Montoneri, E.; Bottigliengo, S.; Boffa, V.; Guizzetti, T.; Perrone, D.G.; Mendichi, R. Biosurfactants from urban wastes as auxiliaries for textile dyeing, Ind. Eng. Chem. Res. **2009,** *48*, 3738-3748.

58. Speziale, S.; Duffy, T. S. Single-crystal elastic constants of fluorite (CaF$_2$) to 9.3 GPa, *Phys. Chem. Minerals*, **2002**, *29*, 465-472.

59. Ondrus, P.; Veselovsky, F.; Gabasova, A.; Hlousek, J.; Srein, V.; Vavrnn, I.; Skala, R.; Sejkora, J.; Drabek, M. Primary minerals of the Jáchymov ore district, Journal of the Czech Geological Society, **2003**, *48*, 19-147.

60. Paquette, J.; Reeder, R. J. Single-crystal X-ray structure refinements of two biogenic magnesian calcite crystals *Am. Mineralogist*, **1990**, *75*, 1151-1158.

61. Gupta, A.K. S. Ion Exchange in Environmental Processes: Fundamentals, Applications and Sustainable Technology, First Edition. **2017** John Wiley & Sons, Inc.

1
2
3
4
5
6
7
8
9
10
11
12
13
14
15
16
17
18
19
20
21
22
23
24
25
26
27
28
29
30
31
32
33
34
35
36
37
38
39
40
41
42
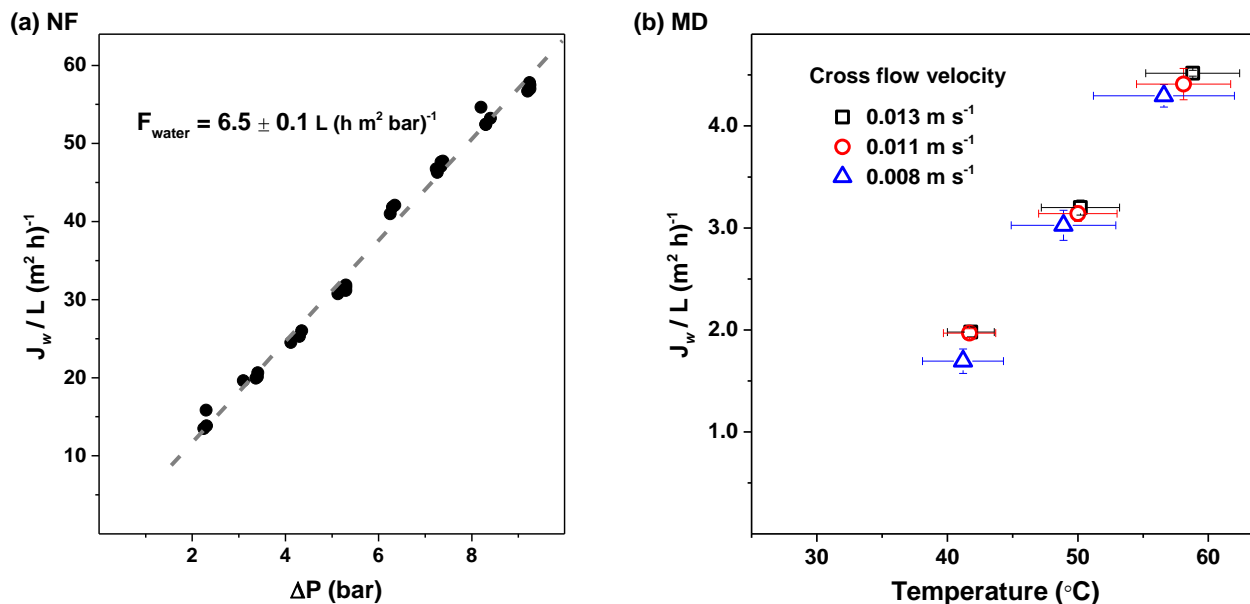43
44
45
46
47
48
49
50
51
52
53
54
55
56
57
58
59
60

1
2
3
4
5
6
7
8
9
10
11
12
13
14
15
16
17
18
19
20
21
22
23
24
25
26
27
28
29
30
31
32
33
34
35
36
37
38
39
40
41
42
43
44
45
46
47
48
49
50
51
52
53
54
55
56
57
58
59
60

Table of Contents Graphic
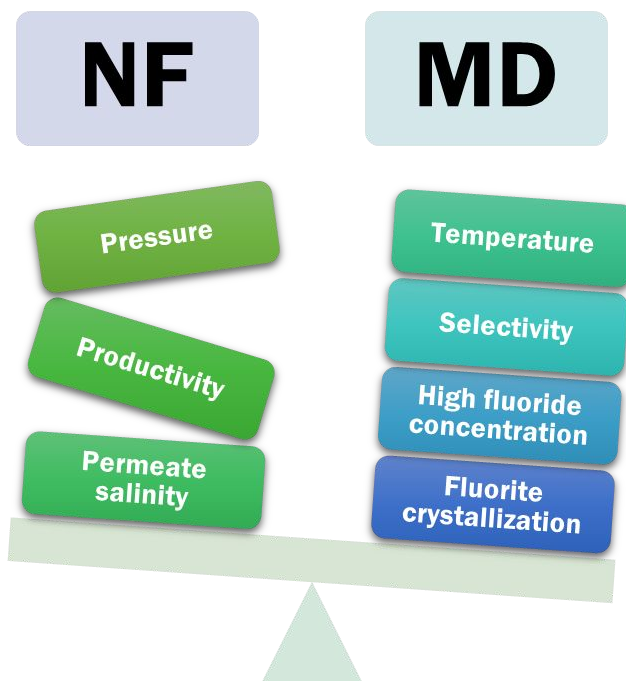
Figures

Figure 1. Filtration of deionized water. (a) Permeate flux (J_w) as a function of membrane overpressure in NF; the linear fitting of the experimental data (dashed line) was used to calculate the membrane water permeance (F_{water}). (b) J_w of MD as a function of feed temperature: the horizontal bars and bullets indicate the temperature at the two membrane extremes and the average temperature, respectively; vertical bars indicate the standard deviation over 4 measurements; the permeate had an average temperature of 20 °C and the same cross flow velocity of the feed.

1
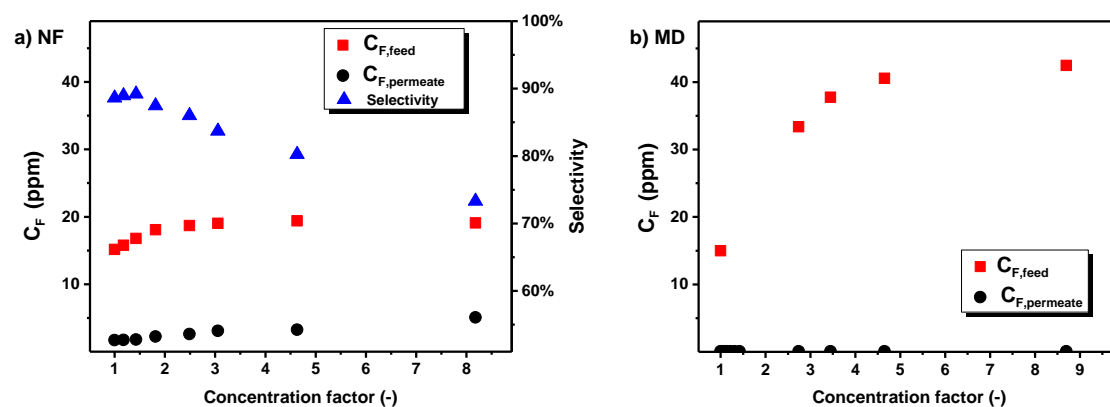
Figure 2. Fluoride concentration in the feed and in the permeate during concentration of the model water system in Table 1. (a) Nanofiltration (NF) was performed at ΔP = 9 bar, cross flow rate of 0.17 L s^{-1}. (b) Membrane distillation (MD) was performed at a cross-flow velocity of 0.013 m s^{-1} and the average temperatures of the feed side and side were 58 °C and 20 °C, respectively; the initial volumes of feed and permeate were 2.4 L and 0.40 L, respectively.
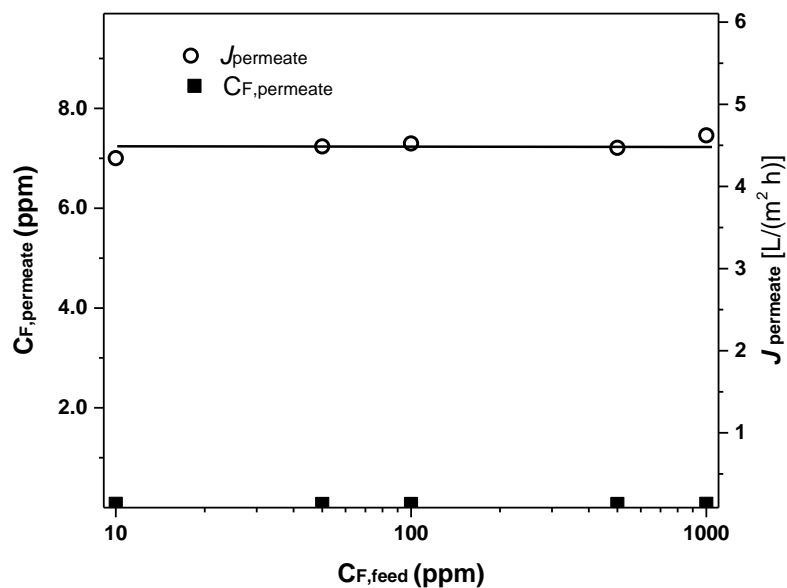
Figure 3. Filtration of deionized water contaminated with fluorine: measured fluoride concentration in the permeate ($C_{F,permeate}$) and permeate flux (J_W) as a function of the fluoride concentration in the feed tank ($C_{F,feed}$) for the MD membrane. The experiment was performed at a cross-flow velocity of 0.013 m s^{-1} and the average temperatures of the feed side and permeate side were 58 °C and 20 °C, respectively; the initial volumes of feed and permeate were 2.4 L and 0.40 L, respectively.

3
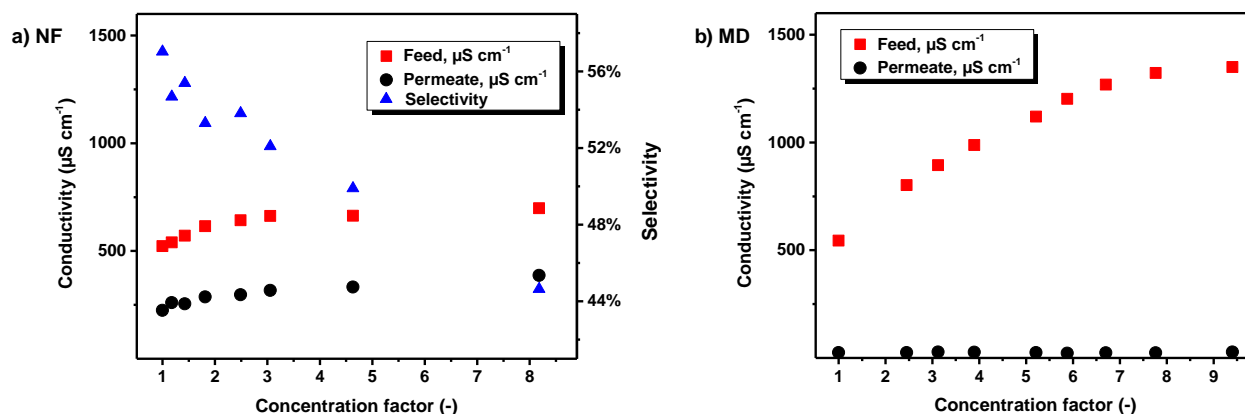
Figure 4. Conductivity of the feed and of the permeate during concentration of the model water system in Table 1. (a) Nanofiltration (NF) was performed at $\Delta P = 9$ bar and crossflow rate of 0.17 L s^{-1}. (b) Membrane distillation (MD) was performed at a cross-flow velocity of 0.013 m s^{-1} and the average temperatures of the feed side and permeate side were 58 °C and 20 °C, respectively; the initial volumes of feed and permeate were 2.4 L and 0.40 L, respectively.
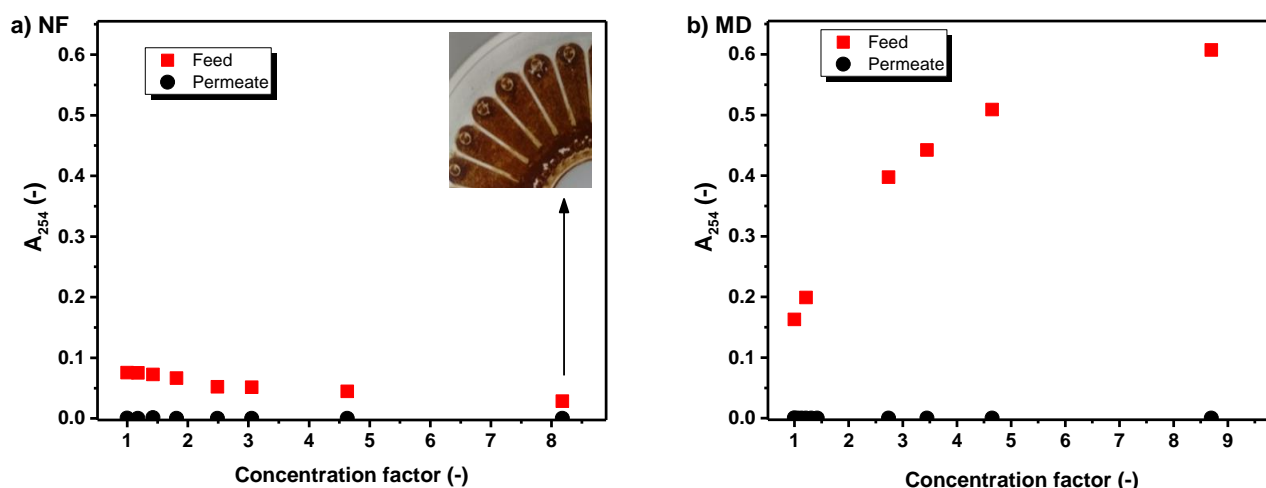
Figure 5. Light absorbance at 254 nm (A_{254}) of the feed and of the permeate during concentration of the model water system in Table 1. (a) Nanofiltration (NF) was performed at $\Delta P = 9$ bar, cross flow rate of 0.17 L s^{-1}; the picture in the insert shows a portion of the surface of the polymeric NF membrane at the end of the experiment. (b) Membrane distillation (MD) was performed at a cross-flow velocity of 0.013 m s^{-1} and the average temperatures of the feed side and permeate side were 58 °C and 20 °C, respectively; the initial volumes of feed and permeate were 2.4 L and 0.40 L, respectively.
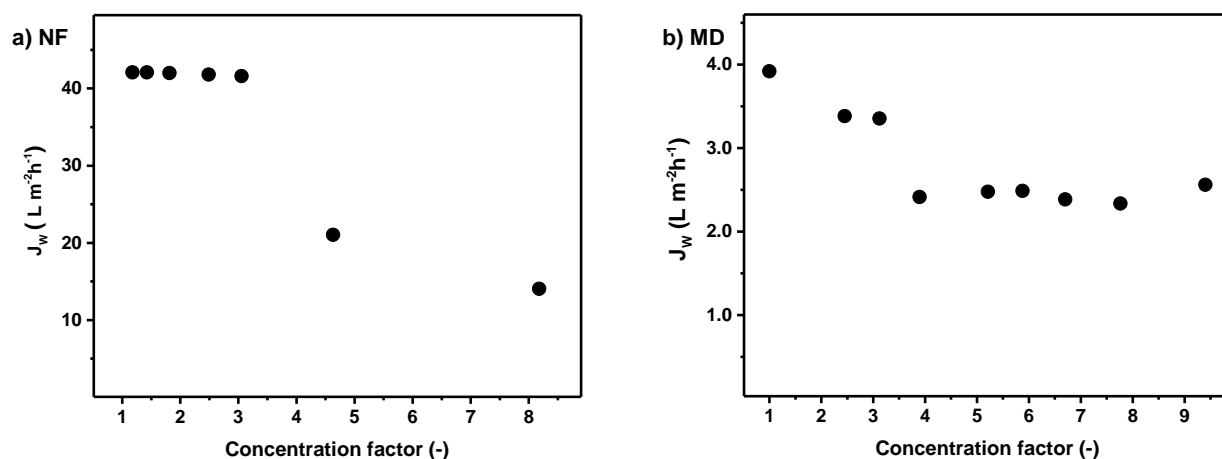
5

Figure 6. Permeate flux (J_w) during concentration of the model water system in Table 1. (a) Nanofiltration (NF) was performed at $\Delta P = 9$ bar, cross flow rate of 0.17 L s^{-1}; the picture in the insert shows a portion of the surface of the polymeric NF membrane at the end of the experiment. (b) Membrane distillation (MD) was performed at a cross-flow velocity of 0.013 m s^{-1} and the temperatures of the feed side and permeate side were 58 °C and 20 °C, respectively; the initial volumes of feed and permeate were 2.4 L and 0.40 L, respectively.
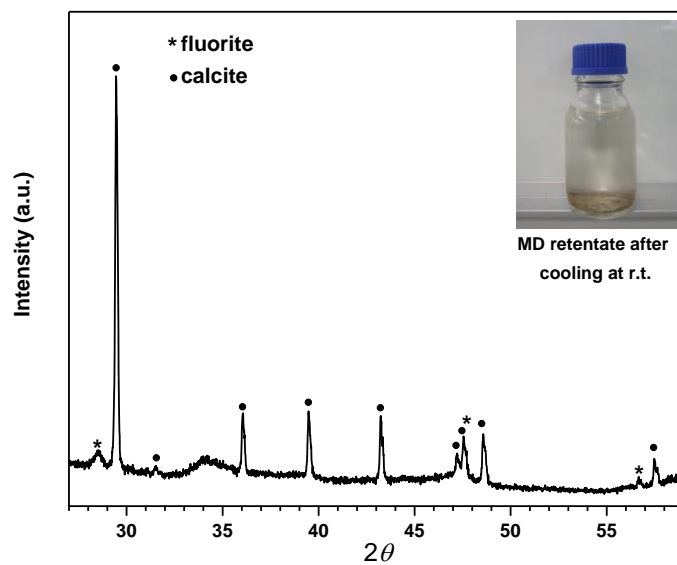
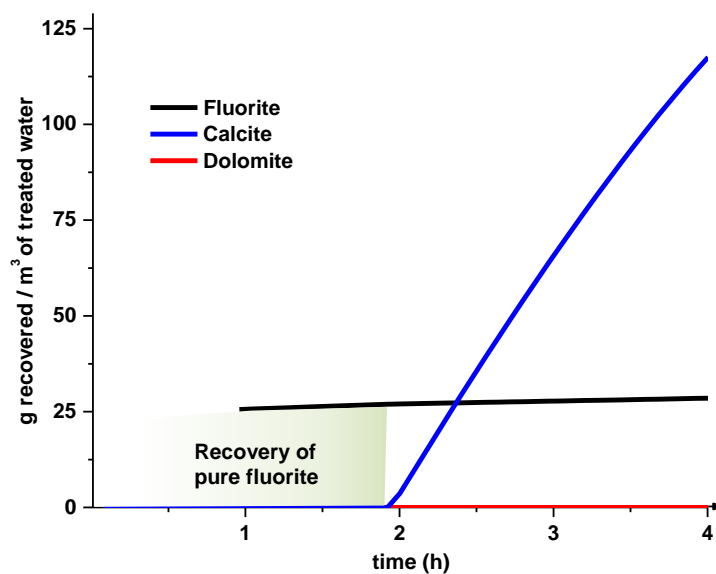Figure 7. XRD pattern of the crystals in the MD concentrate, which showed in the insert picture.

Figure 8. MD can be used to recover pure fluorite upon partial concentration of fluoride-contaminated water. The *x*-axes indicates the filtration time for 1 m^3 of a fluoride-contaminated water (Table 1) over a MD membrane of the same type which was used in our experiment and an area of 50 m^2. The *y*-axes indicates the amount of salt the can be recovered from the concentrate.

8